PERGAMON

International Journal of Heat and Mass Transfer 45 (2002) 319–329

International Journal of HEAT and MASS TRANSFER

www.elsevier.com/locate/ijhmt

Laminar free convection from a vertical plate with uniform surface heat flux in chemically reacting systems

C. Cianfrini, M. Corcione *, D.M. Fontana

Dipartimento di Fisica Tecnica, University of Rome "La Sapienza", via Eudossiana 18, 00184 Rome, Italy

Received 8 May 2000; received in revised form 12 April 2001

Abstract

Two-dimensional steady laminar free convection from a vertical plate with uniform surface heat flux rate is studied in a gas where a reversible very fast reaction of dissociation $A \leftrightarrow 2B$ takes place at atmospheric pressure. The effective thermophysical properties of the gas in the interval of dissociation are evaluated and the governing boundary-layer equations are solved numerically by a finite-difference method with control volume formulation for a wide range of values of the independent variables which have a significant influence on the phenomenon. In the case of undisturbed fluid temperature T_∞ smaller than $T_{0.5}$, corresponding to a rate of dissociation $\alpha = 0.5$, three different heat transfer regimes, marked by two critical heat fluxes, may be distinguished as the surface heat flux rate increases. The theoretical results obtained for the critical heat fluxes as well as the coefficient of convection are expressed in terms of correlations among dimensionless parameters defined through the mixture effective properties.

Keywords: Laminar free convection; Uniform heat flux; Dissociated gases; Dimensionless correlations

1. Introduction

In systems where a chemical reaction of dissociation–recombination takes place, the total heat transfer may be increased owing to the energy transfer by diffusion under the influence of a concentration gradient.

Most of the previous work on this subject has been developed in the fields of combustion [1–9], rocket propulsion [10–13], hypersonic flows and atmospheric re-entry problems [1,14–17], essentially with reference to forced convection.

Leaving aside a small number of papers which consider the effects of finite chemical reaction times [2,3,7,9,14], the majority of them assume both hypotheses of fast chemistry and that the flow in the boundary layer is in thermodynamic equilibrium. That is to say, they assume that the reaction times are very short in comparison with the time rates of diffusion and convection through the boundary layer as well as that the products of the fast chemistry are the equilibrium products, thus following that either the temperature or concentration distribution along with the pressure is a sufficient description of the thermodynamic state of the boundary layer.

Free convection heat transfer in chemically reacting gases seems to be investigated only for laminar flames [5–8], whose study has however been conducted by neglecting any dissociation effect on physical properties.

Actually, since dissociation has a direct influence on gas density and then the related buoyancy forces, in free convection the chemical reactions greatly affect both heat transfer effectiveness and the flow driving forces.

In a previous work, the same authors of the present paper analyzed the laminar free convection heat transfer from an isothermal vertical plate in partly dissociated gases under the assumption of very fast chemistry and migration to products of complete chemical equilibrium [20], showing that the results obtained could be correlated by the following equation:

* Corresponding author.

0017-9310/02/$ - see front matter
PII: S0017-9310(01)00144-2

Nomenclature

A, B	chemical species
C_P	specific heat at constant pressure
D	coefficient of diffusion
g	gravitational constant
h	local heat transfer coefficient
$\overline{h}$	average heat transfer coefficient
H	specific enthalpy
J	specific flux of matter with respect to mass average velocity
K	equilibrium constant
L	height of the wall
M	molecular weight
P	pressure
q	specific heat flux
R_0	constant of gases
T	absolute temperature
$T_{0.05}$, $T_{0.5}$, $T_{0.95}$	temperature corresponding to a dissociation rate $\alpha = 0.05$, 0.5, 0.95
u	axial velocity component
v	normal velocity component
x	longitudinal coordinate
y	normal coordinate
ΔH	heat of dissociation
$\Delta T_{0.9}$	$= T_{0.95} - T_{0.05}$
Q	dimensionless specific heat flux
Nu	Nusselt number
Pr	Prandtl number
Gr	Grashof number
$Gr(q)$	thermal flux Grashof number

Greek symbols

α	fraction of dissociated moles of gas A
λ	thermal conductivity
ε	standard deviation
η	relative error
ξ	longitudinal coordinate
ω	normal coordinate
θ	dimensionless average wall–fluid temperature difference
μ	dynamic viscosity
$\tilde{\chi}$	mole fraction
ρ	mass density

Subscripts

A, B, i, j	refers to species A and B
CR1, CR2	refers to critical heat fluxes
FR	refers to the frozen mixture
max	maximum value
M	refers to the grid node of the ω-direction spacing corresponding to $\omega = 1$
ref, r	reference
T_{ref}	at the reference temperature T_{ref}
T_r	at the reference temperature T_r
$T_{0.5}$	at the temperature corresponding to $\alpha = 0.5$
x	relevant to the x-coordinate
W	at the wall surface
∞	far from the wall surface

Superscript

$*$	refers to the chemically reacting system (“effective” property)

$$Nu_W = 0.52(Gr^*_\infty)^{0.25}(Pr^*_\infty)^{0.33}\left(\frac{Pr^*_W}{Pr^*_\infty}\right)^{0.55}\left(\frac{\rho_W}{\rho_\infty}\right)^{-0.2}, \quad (1)$$

where the dimensionless parameters are defined through the mixture effective properties calculated at the wall temperature T_W as well as the undisturbed fluid temperature T_∞.

In the present paper, the study of the laminar boundary layer is presented for uniform heat flux rate at the surface of the vertical plate, again under the assumption of fast reaction times and migration to products of chemical equilibrium. In this case, while the numerical method of solution of the governing equations of mass, momentum and energy conservation is almost the same as that adopted for uniform surface temperature, much more efforts are required for data correlation. This is due to the strict relationship between the fluid effective properties, which vary largely with temperature in the interval of dissociation, and the boundary layer temperature distribution, not known a priori and, in turn, largely depending on the effective properties themselves.

2. Theoretical analysis

Two-dimensional steady free convection from a vertical plate with uniform surface heat flux q_W is studied in a gas where a reversible very fast reaction of dissociation $A \leftrightarrow 2B$ takes place at atmospheric pressure, assuming that chemical equilibrium prevails throughout.

Both A and B are treated as perfect gases with constant physical properties except density. Laminar boundary-layer flow is assumed. Viscous dissipation, work against gravity field and thermal diffusion are neglected. The undisturbed fluid temperature T_∞ outside the boundary layer as well as the pressure P throughout the boundary layer is assumed uniform.

3. Effective properties

In the presence of a dissociation–recombination reaction, modifications of the gas thermophysical properties occur due to the following main reasons: (a) the

system consists of two different chemical species; (b) energy transfer by diffusion and recombination processes may appreciably add to the heat transferred by normal molecular conduction.

In the present paper, effective viscosity, density, coefficient of thermal expansion and specific heat at constant pressure are evaluated by taking into account only the first effect, while effective conductivity is calculated by considering both effects.

3.1. Viscosity μ^*

The effective viscosity is evaluated with reference to a "frozen" (namely, non-reacting) mixture of perfect gases, according to Wilke's relations [18]:

$$\mu^* = \mu_{\mathrm{FR}} = \sum_i \frac{\mu_i \tilde{\chi}_i}{\sum_j \tilde{\chi}_j \phi_{ij}} \quad (i = A, B \text{ and } j = A, B) \tag{2}$$

with

$$\phi_{ij} = \frac{\left[1 + \left(\frac{\mu_i}{\mu_j}\right)^{1/2} \left(\frac{M_j}{M_i}\right)^{1/4}\right]^2}{\left[8\left(1 + \frac{M_i}{M_j}\right)\right]^{1/2}} \quad (i = A, B \text{ and } j = A, B), \tag{3}$$

where μ_i (or μ_j), $\tilde{\chi}_i$ (or $\tilde{\chi}_j$) and M_i (or M_j) are, respectively, the viscosity, the mole fraction and the molecular weight of the ith (jth) component of the mixture.

3.2. Conductivity λ^*

By introducing the frozen thermal conductivity of the mixture, still defined according to Wilke:

$$\lambda_{\mathrm{FR}} = \sum_i \frac{\lambda_i \tilde{\chi}_i}{\sum_j \tilde{\chi}_j \phi_{ij}} \quad (i = A, B \text{ and } j = A, B), \tag{4}$$

where λ_i is the thermal conductivity of the ith component of the mixture and ϕ_{ij} is given by Eq. (3), the total heat flux q_x at a distance x from the leading edge of the plate is obtained by the sum of the contributions due to thermal conduction and the diffusion–recombination process:

$$q_x = -\lambda_{\mathrm{FR}} \frac{\partial T}{\partial y} + J_B \Delta H, \tag{5}$$

where $\partial T/\partial y$ is the local value of the temperature gradient normal to the plate, J_B is the specific mass flow of B and ΔH is the heat of dissociation.

Since the type of diffusion involved is neither equimolal nor diffusion through a stagnant film, J_B may be expressed through the general form of Fick's law [13]:

$$J_B = -M_B D_{BA} \frac{\rho_A}{M_A} \frac{1/2}{1 - (\alpha/2)} \frac{\partial \alpha}{\partial y}, \tag{6}$$

where D_{BA} is the coefficient of diffusion of B through A, α is the fraction of dissociated moles of A and ρ_A is the density of gas A undissociated.

Under the assumption of chemical equilibrium mentioned above, α is a function of the sole temperature, thus following that:

$$\frac{\partial \alpha}{\partial y} = \frac{\mathrm{d}\alpha}{\mathrm{d}T} \frac{\partial T}{\partial y} \tag{7}$$

and, since reactions of the kind $A \leftrightarrow 2B$ are considered thus resulting: $M_B/M_A = 1/2$, by combining Eqs. (5)–(7), the effective total conductivity may then be derived:

$$\lambda^* = \lambda_{\mathrm{FR}} + D_{BA} \rho_A \Delta H \frac{1}{1 - (\alpha/2)} \frac{\mathrm{d}\alpha}{\mathrm{d}T}, \tag{8}$$

where the first term accounts for the molecular collision process and the second term, which could be called reacting conductivity, accounts for heat transfer by the diffusion and recombination of dissociated species.

The expressions of α and $\mathrm{d}\alpha/\mathrm{d}T$ to be introduced in Eq. (8) may be obtained through the van't Hoff equation, as discussed in full detail in [20]:

$$\frac{\mathrm{d}(\ln K_{\mathrm{P}})}{\mathrm{d}T} = \frac{M_A \Delta H}{R_0 T^2} \tag{9}$$

with

$$K_{\mathrm{P}} = \frac{4\alpha^2}{1 - \alpha^2} \frac{P}{P_{\mathrm{ref}}} \tag{10}$$

and

$$\Delta H = \Delta H(T) = \Delta H_{T_{\mathrm{ref}}} + (C_{\mathrm{P}B} - C_{\mathrm{P}A})(T - T_{\mathrm{ref}}), \tag{11}$$

where R_0 is the constant of perfect gases, P is the total pressure of the mixture, P_{ref} is the reference value of pressure (assumed equal to P), T_{ref} is the reference value of temperature and $C_{\mathrm{P}A}$ and $C_{\mathrm{P}B}$ are the specific heats at constant pressure of A and B.

3.3. Density ρ^* and coefficient of thermal expansion β^*

From the state equation for perfect gases, by taking into account that $M_B/M_A = 1/2$, it follows:

$$\rho^* = \frac{P M_A}{R_0} \frac{1}{(1 + \alpha) T} \tag{12}$$

and then

$$\beta^* = -\frac{1}{\rho^*} \left(\frac{\mathrm{d}\rho^*}{\mathrm{d}T}\right). \tag{13}$$

3.4. Specific heat at constant pressure C_{P}^*

From the enthalpy H of the mixture

$$H = (1 - \alpha) C_{\mathrm{P}A} (T - T_{\mathrm{ref}}) + \alpha [C_{\mathrm{P}B} (T - T_{\mathrm{ref}}) + \Delta H] \tag{14}$$

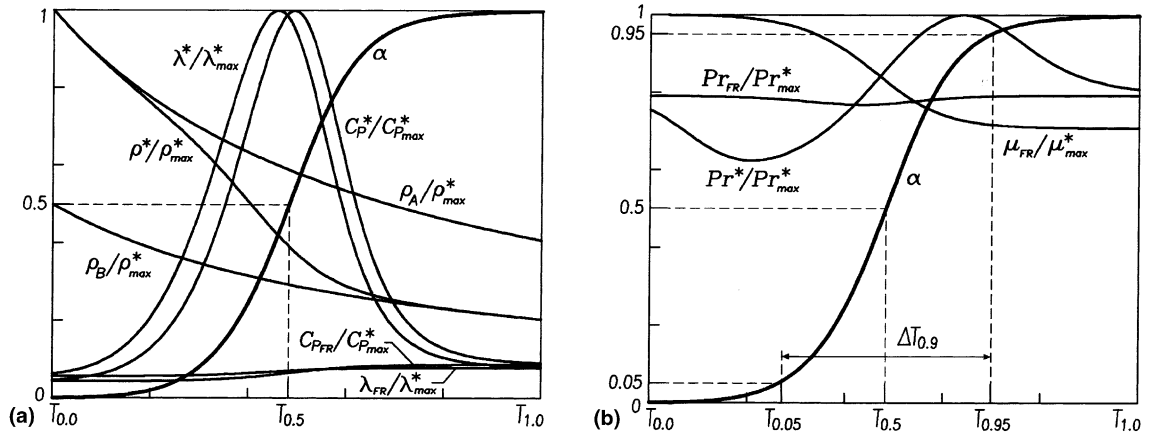

Fig. 1. Distributions of the effective properties vs. temperature in the interval of dissociation.

it follows:

$$C_{\mathrm{P}}^{*}=\frac{\mathrm{d}H}{\mathrm{d}T}=\left[(1-\alpha)C_{\mathrm{P}A}+\alpha C_{\mathrm{p}B}\right]+\Delta H\frac{\mathrm{d}\alpha}{\mathrm{d}T}. \tag{15}$$

Since the pressure P is assumed constant within the boundary layer, the effective properties discussed above are the functions solely of temperature. Fig. 1 shows the typical distributions of α and both the effective and frozen properties with temperature, where the subscript of temperature denotes the dissociation rate. It may be noticed that:

(a) λ^* and C_{P}^* undergo large variations with temperature up to 10 times the frozen values, with a maximum for $\alpha \cong 0.5$;

(b) λ^* and C_{P}^* have similar distributions, so that the variations of the effective Prandtl number Pr^* with temperature are smaller than those corresponding to both λ^* and C_{P}^*;

(c) the variation of ρ^* with temperature is much larger than those corresponding to both ρ_A and ρ_B.

4. Governing equations

The laminar boundary-layer equations for incompressible flow expressed in the (ξ,ω) coordinate system given in Fig. 2:

$$\xi = x \quad \omega = \frac{y}{\Psi}, \tag{16}$$

where $\Psi = \Psi(\xi) = C\xi^b$, with C and b constants, are:

Continuity equation:

$$\frac{\partial \rho^* u}{\partial \xi}+\frac{1}{\Psi}\frac{\partial \rho^* v}{\partial \omega}-\frac{\omega}{\Psi}\frac{\mathrm{d}\Psi}{\mathrm{d}x}\frac{\partial \rho^* u}{\partial \omega}=0. \tag{17}$$

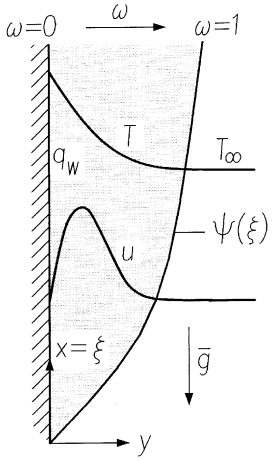

Fig. 2. Physical model coordinate system.

Momentum (*mean mass flow*) *equation*:

$$\rho^* u\frac{\partial u}{\partial \xi}+\left(\frac{\rho^* v}{\Psi}-\rho^* u\frac{\omega}{\Psi}\frac{\mathrm{d}\Psi}{\mathrm{d}x}\right)\frac{\partial u}{\partial \omega}-\frac{1}{\Psi^2}\frac{\partial}{\partial \omega}\left(\mu_{\mathrm{FR}}\frac{\partial u}{\partial \omega}\right)+g(\rho^*-\rho^*_\infty)=0, \tag{18}$$

which, taking into account Eq. (17), becomes

$$\frac{\partial}{\partial \xi}(\rho^* u\Psi u)+\frac{\partial}{\partial \omega}\left[u\left(\rho^* v-\rho^* u\omega\frac{\mathrm{d}\Psi}{\mathrm{d}x}\right)-\frac{\mu_{\mathrm{FR}}}{\Psi}\frac{\partial u}{\partial \omega}\right]+g(\rho^*-\rho^*_\infty)=0. \tag{19}$$

Energy equation:

$$\frac{\partial}{\partial \xi}(\rho^* u\Psi h)+\frac{\partial}{\partial \omega}\left[h\left(\rho^* v-\rho^* u\omega\frac{\mathrm{d}\Psi}{\mathrm{d}x}\right)-\frac{\lambda^*}{\Psi}\frac{\partial T}{\partial \omega}\right]=0 \tag{20}$$

or

$$\frac{\partial}{\partial\xi}(\rho^* u\Psi C_P^* T)+\frac{\partial}{\partial\omega}\left[C_P^* T\left(\rho^* v-\rho^* u\omega\frac{d\Psi}{dx}\right)-\frac{\lambda^*}{\Psi}\frac{\partial T}{\partial\omega}\right]=0. \tag{21}$$

The boundary conditions are derived by imposing a given uniform heat flux rate q_W and zero velocity at the plate surface, as well as zero velocity and velocity gradient, uniform temperature and zero temperature gradient at a great distance from the plate.

Hence,

$$\begin{aligned}&\omega=0;\ \ \xi\geqslant 0:\\ &\quad u=v=0;\quad q=-\lambda\frac{1}{\Psi}\left(\frac{\partial T}{\partial\omega}\right)_{\omega=0}=q_W.\\ &\omega\to\infty;\ \ \xi\geqslant 0:\\ &\quad u=v=0;\quad \frac{\partial u}{\partial\omega}=\frac{\partial v}{\partial\omega}=0;\quad T=T_\infty;\quad \frac{\partial T}{\partial\omega}=0.\end{aligned} \tag{22}$$

5. Method of solution

The set of governing equations (Eqs. (17) and (19)–(22)) has been solved numerically by a finite-difference method with control volume formulation and assuming ξ as a one-way coordinate. In the derivation of the discretized equations, along the ξ-direction the downstream values of the dependent variable are assumed to prevail over the entire $\Delta\xi$ of the control volume, while along the ω-direction the exponential scheme [19] has been considered.

The $\Delta\xi$ intervals have been assumed less than or equal to $\Psi(\xi)/4$. The values of C and b in the $\Psi(\xi)$ expression given in Eq. (16) have been assumed by a trial-and-error procedure so that the thermal and velocity boundary layers were contained in the range $0\leqslant\omega\leqslant 1$. The values corresponding to the case of a fluid with constant properties evaluated at T_∞ have been assumed as first approximation values. The number of grid nodes in the ω-direction has been chosen so that at least 50 grid nodes were contained within both boundary layers. As far as the node-spacing along the ω-direction is concerned, uniform intervals $\Delta\omega$ and $2\Delta\omega$ have been assumed, respectively, for $0\leqslant\omega\leqslant 0.7$ and $0.7<\omega\leqslant 1$.

For each spatial interval in the ξ-direction, both smallness of values and flatness of T and u profiles have been verified through

$$\begin{aligned}&|T_M-T_\infty|\leqslant|T_W-T_\infty|\times 10^{-3},\\ &\quad u_M\leqslant u_{max}\times 10^{-3}\\ &|T_M-T_{M-1}|\leqslant|T_W-T_\infty|\times 10^{-4},\\ &\quad |u_M-u_{M-1}|\leqslant u_{max}\times 10^{-4}\end{aligned} \tag{23}$$

where subscript max refers to the maximum value in the boundary layer, while subscript M refers to the grid node of the ω-direction spacing corresponding to $\omega=1$.

Owing to the strong non-linearities essentially due to the effect of temperature on dissociation and then on the fluid physical properties, within each discretization step along the ξ-direction iterations have been executed on temperature and velocity fields up to convergence attainment. Furthermore, the local value of the gradient $\partial T/\partial\omega$ has been evaluated by a second-order interpolation.

6. Heat transfer features

A series of preliminary tests has been carried out in order to point out the influence of the surface heat flux rate on heat transfer efficiency. It has been found that, for undisturbed fluid temperatures T_∞ smaller than $T_{0.5}$ corresponding to a rate of dissociation $\alpha=0.5$, the relationship between the surface heat flux rate q_W and the dimensionless average temperature difference between wall and fluid $\overline{\theta}=(\overline{T}_W-T_\infty)/(T_{0.5}-T_\infty)$ is represented by curves of the kind shown in Fig. 3, where the distributions of the local values of $\theta=(T_W-T_\infty)/(T_{0.5}-T_\infty)$ vs. $\xi=x$ for several values of q_W are also represented.

The peculiar shape of the curve q_W vs. $\overline{\theta}$ displays three regions corresponding to different heat transfer regimes as the surface heat flux rate q_W increases.

In region (I), $\overline{\theta}$ increases gradually with a decreasing slope and related increasing values of the average coefficient of heat transfer $\overline{h}=q_W/(\overline{T}_W-T_\infty)$ of the order of 10^2. Regime (I) occurs as T_W is smaller than about $T_{0.5}(\theta<1)$ along the entire length of the wall, that is to say that the rate of dissociation α at any point within the boundary layer is smaller than 0.5, thus following that, according to Fig. 1, the effective conductivity λ^*, and then h, increase with temperature. Regime (I) expires as T_W reaches about $T_{0.5}(\theta\cong 1)$ at the end of the plate, at a critical value q_{CR1} of the surface heat flux rate over which changes in heat transfer features are detected.

In region (II), which represents what might be called a transition regime, the average wall–fluid temperature difference shows a steep increase, with corresponding decreasing values of the average coefficient of heat transfer $\overline{h}$ in the range 10^2–10^0. This is due to the abrupt increase of T_W above $T_{0.5}$ (θ above 1) which occurs when $q_W>q_{CR1}$ as a strict consequence of the fact that, according to Fig. 1, λ^*, and then h, decrease with temperature, thus resulting: $\partial[h(T_W-T_\infty)]/\partial T_W<0$. Since the heat to be transferred to the fluid is assigned, as q_W continues to increase, large rises in the wall temperature take place up to verifying $\partial[h(T_W-T_\infty)]/\partial T_W>0$ and $h(T_W-T_\infty)=q_W$. This is obtained when the gas in the

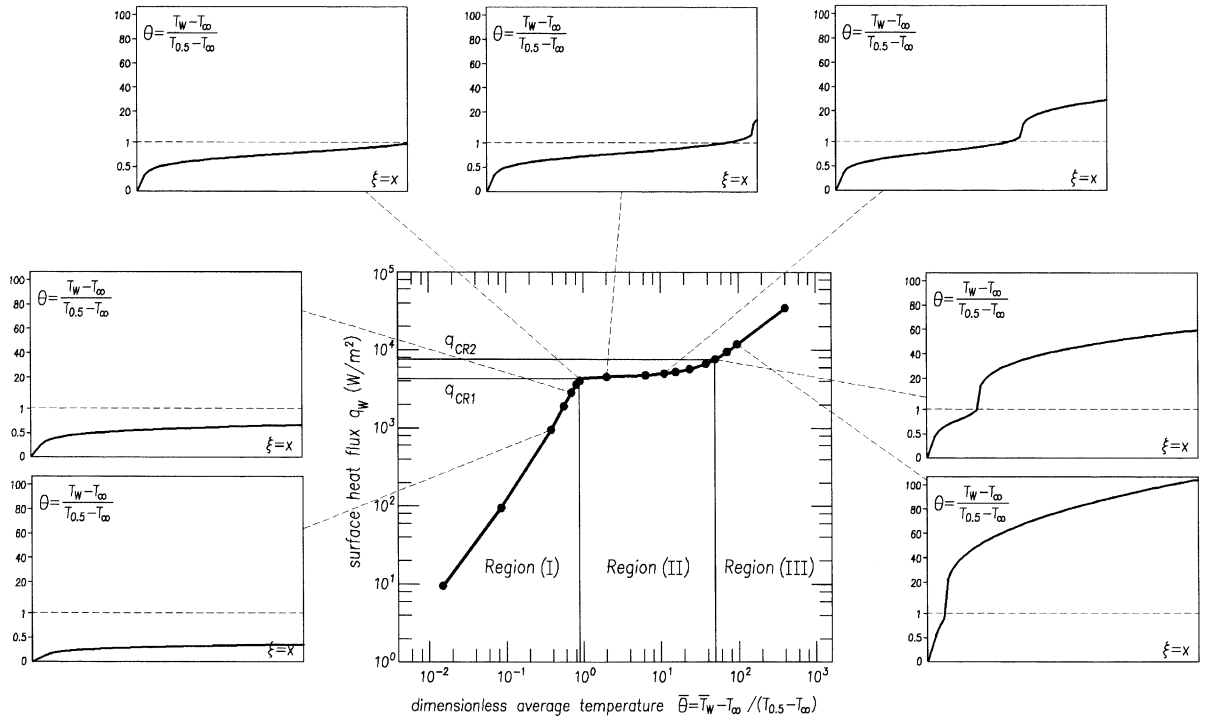

Fig. 3. Relationship between the surface heat flux rate q_W and the dimensionless average wall–fluid temperature difference $\overline{\theta}$.

proximity of the wall is practically completely dissociated ($\alpha_W \cong 1$). The extent of the portion of the plate corresponding to the increase of T_W above $T_{0.5}$ increases as q_W increases and the value of $\overline{h}$ is obtained from the weighted average of the local values of the coefficient of convection above and below the discontinuity point.

When the portion of the plate above the discontinuity point (T_W well above $T_{0.5}$) is larger than approximately the 90% of the total length of the wall, its influence becomes predominant and the average wall–fluid temperature difference resumes its gradual increase, with values of $\overline{h}$ of the order of 10^0. This corresponds to regime (II) expiration, occurring at a critical value q_{CR2} of the surface heat flux rate.

In region (III) most of the boundary layer consists of completely dissociated gas and the distribution of $\overline{\theta}$ vs. q_W is quite similar to that of a non-reacting fluid. In this regard, it is worthwhile noticing that in the analytical approach the condition of completely dissociated gas is never verified since at $\xi = x = 0$ is $T_W = T_\infty < T_{0.5}$. Thus, whatever value of q_W is assumed, the first portion of the boundary layer is always consisting of partly dissociated gas. In the numerical scheme, on the contrary, this condition may be already encountered at the first discretization step along the wall (namely, at the leading edge of the plate), when sufficiently large heat flux rates are considered.

As far as the increases of temperature T_W along the plate consequent to the increase in boundary layer thickness are concerned, it may be observed that:
(a) in region (I) they are smaller than those corresponding to the case of a gas with constant physical properties due to the increase in h consequent to the increase in λ^*;
(b) in region (II) they are practically discontinuous, with a sudden increase of T_W above $T_{0.5}$ occurring at a distance from the leading edge of the plate which decreases as the heat flux rate increases;
(c) in region (III), for most of the wall, they are very similar to those for a non-reacting gas.

Therefore, in both regimes (I) and (III) the increases of T_W vs. $\xi = x$ are relatively small and smooth enough to assume that, once the the values of the two critical heat fluxes q_{CR1} and q_{CR2} are determined, the average coefficient of convection $\overline{h}$ may be expressed through correlations not too different from those commonly used in the case of free convection heat transfer in non-reacting systems from vertical plates with uniform surface heat flux [21].

7. Numerical simulations and heat transfer analysis

The employment of Eqs. (2)–(15) has allowed us to reduce the phenomenon here analyzed to a free con-

vection boundary-layer flow and heat transfer, where the fluid physical properties are the effective properties. The temperature and velocity fields have been solved for a wide range of values of the following independent variables which have a significant influence on the effects pertaining to dissociation:

$2.8 \times 10^{-6} \leqslant D_{BA} \leqslant 2.5 \times 10^{-5}$	(m^2/s)
$200 \leqslant \Delta H(T_{ref} = 298\ K) \leqslant 1900$	(kJ/kg)
$220 \leqslant T_{0.5} \leqslant 1400$	(K)
$2 \times 10^{-23} \leqslant K_p(T_{ref} = 298\ K) \leqslant 4 \times 10^8$	(dimensionless)
$T_{0.5} - 3\Delta T_{0.99} \leqslant T_\infty \leqslant T_{0.5} + 3\Delta T_{0.99}$	(K)

thus resulting in

$4 \times 10^{-3} \leqslant \rho^* \leqslant 9$	(kg/m^3)
$361 \leqslant C_P^* \leqslant 109,000$	(J/kg/K)
$9.2 \times 10^{-3} \leqslant \lambda^* \leqslant 3.2$	(W/m/K)
$1.3 \times 10^{-5} \leqslant \mu^* = \mu_{FR} \leqslant 2.1 \times 10^{-5}$	(Pa s)
$0.5 \leqslant \mid T_W - T_\infty \mid \leqslant 1420$	(K)
$0.18 \leqslant Pr^* \leqslant 4.4$	(dimensionless)

Two kinds of gases are studied:

- A, biatomic, $M_A = 32$ and B, monoatomic, $M_B = 16$ (as for $O_2 \leftrightarrow 2O$),
- A, poliatomic, $M_A = 92$ and B, poliatomic, $M_B = 46$ (as for $N_2O_4 \leftrightarrow 2NO_2$).

The relevant values of C_P have been assumed as for perfect gases, while the values of λ and μ for the dissociated species have been derived from those corresponding to the undissociated species assumed as proportional to $M^{1/2}$ [18].

For each gas the following computational procedure has been followed:

1. select randomly a value of D_{BA}, $\Delta H(T_{ref})$, $T_{0.5}$ and T_∞ in the appropriate ranges and derive the related value of K_P;
2. select randomly a first tentative value of the distance L_0 from the leading edge of the plate corresponding to the abrupt increase of T_W above $T_{0.5}$;
3. solve the governing equations, thus obtaining the thermal and fluid-dynamic fields;
4. find the value of the critical heat flux rate q_{CR1} that gives rise to the sudden increase of T_W above $T_{0.5}$ at a distance ξ^* from the leading edge of the plate in the range $0.9L_0 \leqslant \xi^* \leqslant L_0$;
5. check that at $\xi = \xi^*$ the $\Delta\xi$ discretization step is less than 1% of ξ^*;
6. assume $L_{CR1} = \xi^* - \Delta\xi$ as the "critical" distance from the leading edge of the plate, below which the gas in the boundary layer is still partly dissociated;
7. evaluate the local value h of the coefficient of convection as well as its average value $\overline{h}$ over a portion of plate of length L by

$$h = \frac{q_W}{(T_W - T_\infty)} \tag{24}$$

and

$$\overline{h} = q_W \Big/ \left[\frac{1}{L}\int_0^L (T_W - T_\infty)dx\right]. \tag{25}$$

8. Critical heat flux q_{CR1} correlations

Once the dimensionless critical heat flux Q_{CR1} is introduced,

$$Q_{CR1} = \frac{q_{CR1}L_{CR1}}{\lambda_\infty^*\Delta T_{0.9}} \tag{26}$$

the most suitable correlation among dimensionless parameters has proved to be

$$Q_{CR1} = C(Gr^*_{T_{0.5}})^m(Pr^*_{T_{0.5}})^n\left(\frac{\lambda^*_{T_{0.5}}}{\lambda^*_\infty}\right)^p\left(\frac{\rho^*_{T_{0.5}}}{\rho^*_\infty}\right)^q \times \left(\frac{\Delta T_{0.9}}{T_{0.5} - T_\infty}\right)^r\left(\frac{T_{0.5}}{T_\infty}\right)^s, \tag{27}$$

where

$$Gr^*_{T_{0.5}} = \frac{g\beta^*_{T_{0.5}}(T_{0.5} - T_\infty)L^3_{CR1}}{\nu^{*2}_{T_{0.5}}};$$
$$Pr^*_{T_{0.5}} = \frac{C^*_{PT_{0.5}}\mu^*_{T_{0.5}}}{\lambda^*_{T_{0.5}}}. \tag{28}$$

The values of C, m, n, p, q, r, s have been calculated by the least-squares method through a logarithmic multiple regression. The best fit of data has been obtained with the following correlation, as given in Fig. 4:

$$Q_{CR1} = 1.053(Gr^*_{T_{0.5}})^{0.251}(Pr^*_{T_{0.5}})^{0.387}\left(\frac{\lambda^*_{T_{0.5}}}{\lambda^*_\infty}\right)^{0.924} \times \left(\frac{\rho^*_{T_{0.5}}}{\rho^*_\infty}\right)^{1.35}\left(\frac{\Delta T_{0.9}}{T_{0.5} - T_\infty}\right)^{-0.944}\left(\frac{T_{0.5}}{T_\infty}\right)^{1.73} \tag{29}$$

with $T_{0.5} - 2\Delta T_{0.9} \leqslant T_\infty \leqslant T_{0.5} - 0.1\Delta T_{0.9}$; number of data $N_{data} = 442$; standard deviation of data $\varepsilon = 0.042$; maximum absolute value of the relative error $|\eta|_{max} = 0.15$; percent rate of data within a $\pm 10\%$ relative error $N_{10\%} = 96.8\%$.

9. Heat transfer correlations in regime (I) below the critical heat flux q_{CR1}

The most suitable correlation among dimensionless parameters has proved to be

$$Nu_\infty = C(Gr^*_\infty)^m\left(Pr^*_{T_{0.5}}\right)^n\left(\frac{q_W L}{\lambda^*_\infty\Delta T_{0.9}}\right)^p\left(\frac{\lambda^*_{T_{0.5}}}{\lambda^*_\infty}\right)^q \times \left(\frac{Pr^*_{T_{0.5}}}{Pr^*_\infty}\right)^r\left(\frac{\Delta T_{0.9}}{T_{0.5} - T_\infty}\right)^s, \tag{30}$$

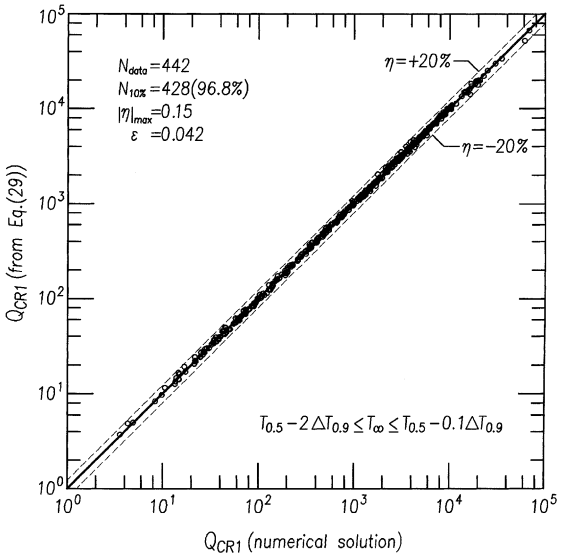

Fig. 4. Comparison between the dimensionless critical heat fluxes Q_{CR1} predicted by Eq. (29) and those derived from the numerical simulations.

where

$$Gr^*_\infty = \frac{g\beta^*_\infty (T_{0.5} - T_\infty)L^3}{\nu^{*2}_\infty}. \tag{31}$$

In order to obtain sufficiently high accuracies, the values of C, m, n, p, q, r, s have been calculated for different ranges of the undisturbed fluid temperature T_∞. The best fit of data has then been obtained with the following correlations, as given, respectively, in Figs. 5–7:

$$Nu_\infty = 0.773(Gr^*_\infty)^{0.177}\left(Pr^*_{T_{0.5}}\right)^{0.253}\left(\frac{q_W L}{\lambda^*_\infty \Delta T_{0.9}}\right)^{0.292} \times \left(\frac{\lambda^*_{T_{0.5}}}{\lambda^*_\infty}\right)^{0.614}\left(\frac{Pr^*_{T_{0.5}}}{Pr^*_\infty}\right)^{-0.106}\left(\frac{\Delta T_{0.9}}{T_{0.5}-T_\infty}\right)^{0.236} \tag{32}$$

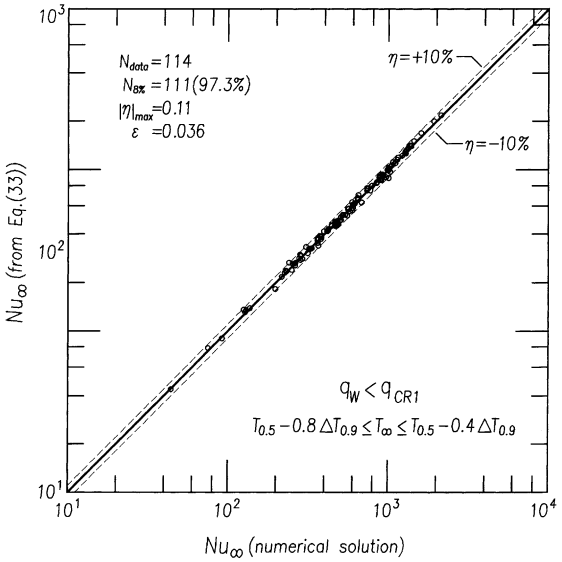

Fig. 6. Comparison between the Nusselt numbers Nu_∞ below the critical heat flux q_{CR1} predicted by Eq. (33) and those derived from the numerical simulations.

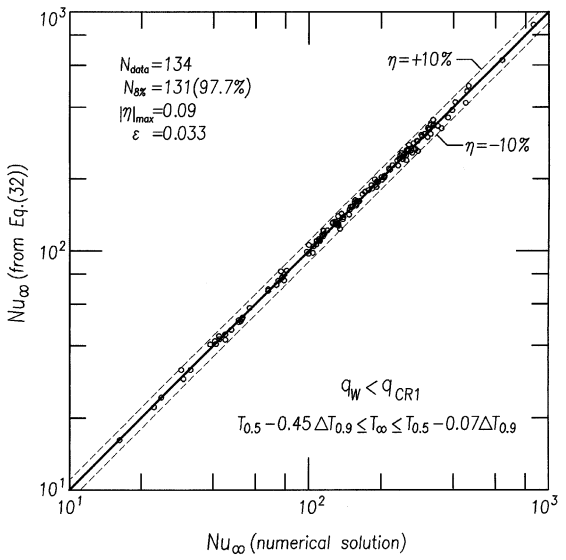

Fig. 5. Comparison between the Nusselt numbers Nu_∞ below the critical heat flux q_{CR1} predicted by Eq. (32) and those derived from the numerical simulations.

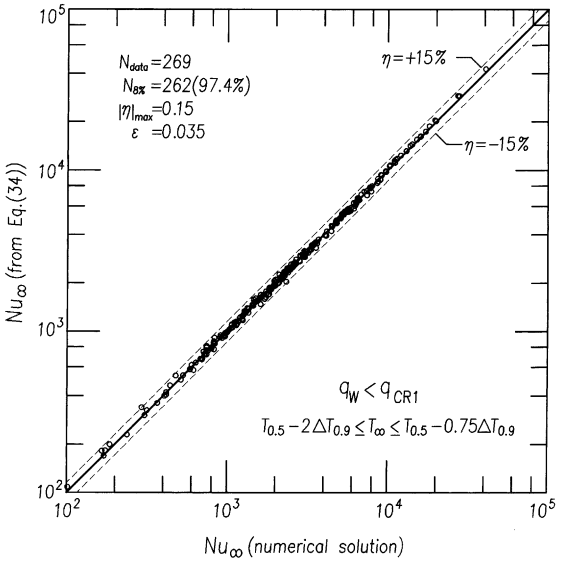

Fig. 7. Comparison between the Nusselt numbers Nu_∞ below the critical heat flux q_{CR1} predicted by Eq. (34) and those derived from the numerical simulations.

with $T_{0.5}-0.45\Delta T_{0.9}\leqslant T_\infty\leqslant T_{0.5}-0.07\Delta T_{0.9}$; number of data $N_{\text{data}}=134$; standard deviation of data $\varepsilon=0.033$; maximum absolute value of the relative error $|\eta|_{\max}=0.09$; percent rate of data within a ±8% relative error $N_{8\%}=97.7\%$,

$$Nu_\infty=0.878(Gr^*_\infty)^{0.120}\left(Pr^*_{T_{0.5}}\right)^{0.163}\left(\frac{q_W L}{\lambda^*_\infty\Delta T_{0.9}}\right)^{0.522}\times\left(\frac{\lambda^*_{T_{0.5}}}{\lambda^*_\infty}\right)^{0.417}\left(\frac{Pr^*_{T_{0.5}}}{Pr^*_\infty}\right)^{0.059}\left(\frac{\Delta T_{0.9}}{T_{0.5}-T_\infty}\right)^{0.530}\tag{33}$$

with $T_{0.5}-0.8\Delta T_{0.9}\leqslant T_\infty\leqslant T_{0.5}-0.4\Delta T_{0.9}$; number of data $N_{\text{data}}=114$; standard deviation of data $\varepsilon=0.036$; maximum absolute value of the relative error $|\eta|_{\max}=0.11$; percent rate of data within a ±8% relative error $N_{8\%}=97.3\%$,

$$Nu_\infty=0.961(Gr^*_\infty)^{0.058}\left(Pr^*_{T_{0.5}}\right)^{0.253}\left(\frac{q_W L}{\lambda^*_\infty\Delta T_{0.9}}\right)^{0.764}\times\left(\frac{\lambda^*_{T_{0.5}}}{\lambda^*_\infty}\right)^{0.256}\left(\frac{Pr^*_{T_{0.5}}}{Pr^*_\infty}\right)^{0.028}\left(\frac{\Delta T_{0.9}}{T_{0.5}-T_\infty}\right)^{1.050}\tag{34}$$

with $T_{0.5}-2\Delta T_{0.9}\leqslant T_\infty\leqslant T_{0.5}-0.75\Delta T_{0.9}$; number of data $N_{\text{data}}=269$; standard deviation of data $\varepsilon=0.035$; maximum absolute value of the relative error $|\eta|_{\max}=0.15$; percent rate of data within a ±8% relative error $N_{8\%}=97.4\%$.

It seems interesting to note that while for non-reacting systems the Nusselt number Nu is usually assumed as proportional to the thermal flux Grashof number $Gr(q)=Gr\times(q_W L/\lambda\Delta T)$, in the present case a better representation of the results is obtained by assuming that Nu depends on Gr and $(q_W L/\lambda\Delta T)$ separately.

10. Critical heat flux q_{CR2} evaluation

As previously described, when the heat flux rate q_W increases above q_{CR1} the abrupt increase of T_W above $T_{0.5}$ which marks the transition regime occurs at a distance L_{CR} from the leading edge of the plate which decreases from the starting value L_{CR1} relevant to q_{CR1}. When q_W reaches the value q_{CR2}, that is to say at the expiration of the transition regime, most of the boundary layer consists of completely dissociated gas and the sudden increase of T_W above $T_{0.5}$ is located at a close distance $L_{CR}=L_{CR2}$ from the leading edge of the plate.

In this regard, the simulations carried out have shown that the beginning of regime (III), namely, when the average wall–fluid temperature difference resumes its gradual increase as q_W continues to increase, is actually obtained when L_{CR2} is of the order of $0.1L_{CR1}$.

It means that, though below L_{CR2} heat transfer occurs in a partly dissociated gas, thus with values of h significantly larger than those pertaining to the completely dissociated gas above L_{CR2}, its influence on the average coefficient of convection $\overline{h}$ is practically negligible.

Herein, by assuming cautiously that L_{CR2} is of the order of $0.01L_{CR1}$, the value of the critical heat flux q_{CR2} is derived from that of q_{CR1} through Eq. (29).

In fact, since q_{CR1} is proportional to $L_{CR1}\times Gr^{*0.251}_{T_{0.5}}$ and then to $L_{CR1}^{(3\times0.251-1)}$, on the assumption that $L_{CR2}=0.01L_{CR1}$, we get $q_{CR2}=q_{CR1}\times0.01^{-0.247}$ and then $q_{CR2}\cong3q_{CR1}$.

11. Heat transfer correlations in regime (III) above the critical heat flux q_{CR2}

The most suitable correlation among dimensionless parameters has proved to be

$$Nu_{T_r}=C(Gr(q)^*_{T_r})^m(Pr^*_{T_r})^n\left(\frac{Pr^*_{T_r}}{Pr^*_\infty}\right)^q\left(\frac{\rho^*_{T_r}}{\rho^*_\infty}\right)^r,\tag{35}$$

where

$$Gr(q)^*=\frac{g\beta^* q_W L^4}{\nu^{*2}\lambda^*}\tag{36}$$

and the thermophysical properties are calculated at a reference temperature T_r.

The best choice for T_r seems to be $\overline{T}_W$, whose value is not known a priori. However, it may be calculated iteratively through $\overline{T}_W=q_W/\overline{h}+T_\infty$, by assuming as first approximation value of $\overline{h}$ that corresponding to a reference temperature $T_r=T_{0.5}+\Delta T_{0.9}$, well beyond the interval of dissociation.

The best fit of data corresponding to the reference temperature $T_r=\overline{T}_W$ is represented by the following correlation, as given in Fig. 8:

$$Nu_{T_r}=0.781(Gr(q)^*_{T_r})^{0.201}\times(Pr^*_{T_r})^{0.4}\left(\frac{Pr^*_{T_r}}{Pr^*_\infty}\right)^{0.014}\left(\frac{\rho^*_{T_r}}{\rho^*_\infty}\right)^{-0.222}\tag{37}$$

with $T_{0.5}-2\Delta T_{0.9}\leqslant T_\infty\leqslant T_{0.5}-0.07\Delta T_{0.9}$; number of data $N_{\text{data}}=297$; standard deviation of data $\varepsilon=0.011$; maximum absolute value of the relative error $|\eta|_{\max}=0.09$; percent rate of data within a ±8% relative error $N_{8\%}=99.3\%$.

In particular, it is worthwhile noticing that the values of the exponents of either the thermal flux Grashof number $Gr(q)$ or the Prandtl number Pr are practically the same as those typical of non-reacting systems (see e.g. [21]).

12. Conclusions

In two-dimensional steady free convection from a vertical plate with uniform surface heat flux q_W in a gas

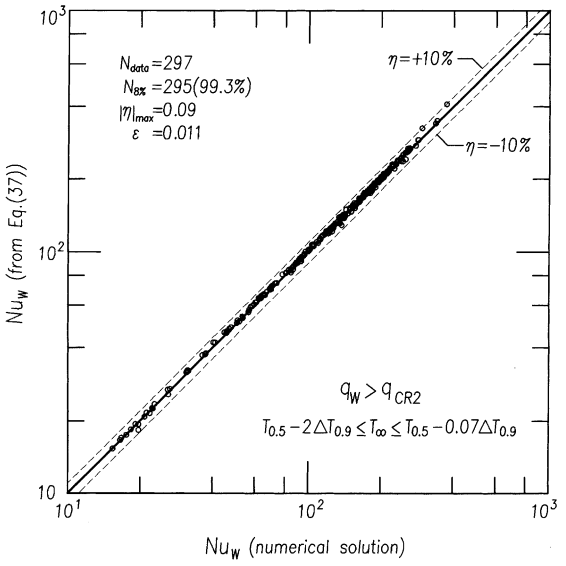

Fig. 8. Comparison between the Nusselt numbers Nu_{T_r} above the critical heat flux q_{CR2} predicted by Eq. (37) and those derived from the numerical simulations.

where a reversible very fast reaction of dissociation $A \leftrightarrow 2B$ takes place at atmospheric pressure, in all those cases wherein $T_\infty < T_{0.5}$ three different heat transfer regimes, marked by two critical heat flux rates q_{CR1} and q_{CR2}, may be distinguished as q_W increases.

In regime (I), occurring as long as $q_W < q_{CR1}$, the average wall temperature increases gradually up to reaching a temperature close to $T_{0.5}$, corresponding to a dissociation rate $\alpha \cong 0.5$, and the average coefficient of convection is of the order of 10^2.

In regime (III), occurring as long as $q_W > q_{CR2}$, the average wall temperature increases gradually well above $T_{0.5}$, the gas is practically completely dissociated and the average coefficient of convection is of the order of 10^0.

In regime (II), occurring as long as $q_{CR1} \leqslant q_W \leqslant q_{CR2}$, the average wall temperature increases abruptly from values typical of regime (I) to values typical of regime (III), with corresponding decreasing values of the average coefficient of convection in the range 10^2–10^0.

Within the bounds of the simulations executed and the approximations introduced, the theoretical results obtained for the critical heat flux rates as well as the coefficients of convection in heat transfer regimes (I) and (III) may be expressed with a sufficiently good accuracy through general correlations among dimensionless parameters not too different from those commonly used for free convection in non-reacting systems from vertical plates with uniform surface heat flux.

References

[1] L. Lees, Laminar heat transfer over blunt bodies at hypersonic flight speeds, Jet Propul. 26 (1956) 259–274.
[2] M. Jischa, An integral method for nonequilibrium dissociating laminar flat plate boundary layer, Int. J. Heat Mass Transfer 15 (1972) 1125–1136.
[3] A. Alkidas, P. Durbetaki, Stagnation point heat transfer: the effect of the first Damkohler similarity parameter, J. Heat Transfer 94 (1972) 410–414.
[4] R. Conolly, R.M. Davies, A study of convective heat transfer from flames, Int. J. Heat Mass Transfer 15 (1972) 2155–2172.
[5] T. Ahmad, G.M. Faeth, An investigation of the laminar overfire region along upright surfaces, J. Heat Transfer 100 (1978) 112–119.
[6] R.J. Neumann, E.W.P. Hahne, Free convective heat transfer to supercritical carbon dioxide, Int. J. Heat Mass Transfer 23 (1980) 1643–1652.
[7] C.H. Chen, J.S. Tien, Fire plume along vertical surfaces: effect of finite rate chemical reactions, J. Heat Transfer 106 (1984) 713–720.
[8] C.P. Mao, A.C. Fernandez-Pello, P.J. Pangi, Mixed convective burning of a fuel surface with arbitrary inclination, J. Heat Transfer 106 (1984) 304–309.
[9] D. Altman, H. Wise, Effect of chemical reactions in the boundary layer on convective heat transfer, Jet Propul. 26 (1956) 256–269.
[10] L.L. Moore, A solution of the laminar boundary layer equations for a compressible fluid with variable properties, including dissociation, J. Aeronaut. Sci. 19 (1952) 505–518.
[11] C.F. Hansen, Note of the Prandtl number for dissociated air, J. Aeronaut. Sci. 20 (1953) 789–790.
[12] H.J. Metzdorf, Flows in partly dissociated gases, J. Aeronaut. Sci. 25 (1958) 200–201.
[13] J.P. Irving, J.M. Smith, Heat transfer in chemically reacting system (nitrogen tetroxide–dioxide), AIChE J. 7 (1961) 91–96.
[14] J.A. Fay, F.R. Riddell, Theory of stagnation point heat transfer in dissociated air, J. Aeronaut. Sci. 25 (1958) 73–121.
[15] P.H. Rose, R.F. Probstein, C. Mac Adams, Turbulent heat transfer through a highly cooled, partially dissociated boundary, J. Aero/Space Sci. 25 (1958) 751–760.
[16] H. Eickhoff, F. Thiele, Influence of the separation of elements on the flow field in hypersonic boundary layers of air in local chemical equilibrium, Int. J. Heat Mass Transfer 18 (1975) 1031–1036.
[17] R.A. East, R.J. Stalker, L.P. Baird, Measurements of heat transfer to a flat plate in a dissociated high-enthalpy laminar flow, J. Fluid Mech. 97 (1980) 673–699.
[18] R.H. Perry, D.W. Green, Perry's Chemical Engineers' Handbook, first ed., McGraw-Hill, Singapore, 1984, p. 279 (Chapter 3).

[19] D.B. Spalding, A novel finite difference formulation for differential expressions involving both first and second derivatives, Int. J. Numerical Meth. Eng. 4 (1972) 551.
[20] D.M. Fontana, M. Corcione, A. Lo Monaco, L. Santarpia, Laminar free convection from a vertical plate in partly dissociated gases, Int. J. Heat Mass Transfer 43 (2000) 1113–1120.
[21] E.M. Sparrow, J.L. Gregg, Laminar free convection from a vertical plate with uniform surface heat flux, ASME Trans. (1956) 435–440.